Research Article

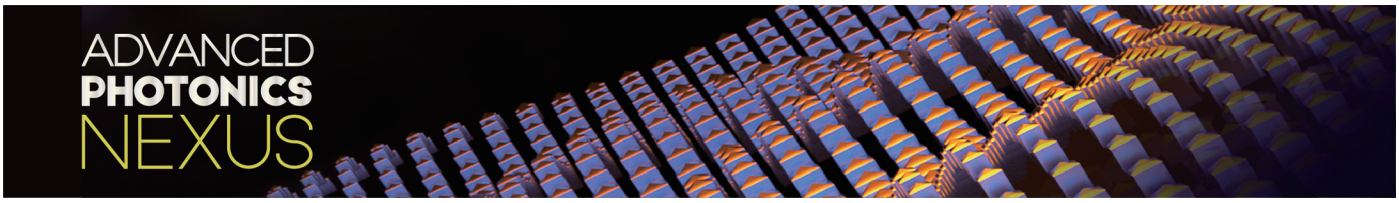

Spectrum shuttle for producing spatially shapable GHz burst pulses

Keitaro Shimada,[a] Ayumu Ishijima,[b,†] Takao Saiki,[b] Ichiro Sakuma,[a,b,c] Yuki Inada,[a,d] and Keiichi Nakagawa[a,b,*]
[a]The University of Tokyo, Department of Bioengineering, Tokyo, Japan
[b]The University of Tokyo, Department of Precision Engineering, Tokyo, Japan
[c]The University of Tokyo, Medical Device Development and Regulation Research Center, Tokyo, Japan
[d]Saitama University, Department of Electronics and Information Sciences, Saitama, Japan

Abstract. Spatiotemporal shaping of ultrashort pulses is pivotal for various technologies, such as burst laser ablation and ultrafast imaging. However, the difficulty of pulse stretching to subnanosecond intervals and independent control of the spatial profile for each pulse limit their advancement. We present a pulse manipulation technique for producing spectrally separated GHz burst pulses from a single ultrashort pulse, where each pulse is spatially shapable. We demonstrated the production of pulse trains at intervals of 0.1 to 3 ns in the 800- and 400-nm wavelength bands and applied them to ultrafast single-shot transmission spectroscopic imaging (4 Gfps) of laser ablation dynamics with two-color sequentially timed all-optical mapping photography. Furthermore, we demonstrated the production of pulse trains containing a shifted or dual-peak pulse as examples of individual spatial shaping of GHz burst pulses. Our proposed technique brings unprecedented spatiotemporal manipulation of GHz burst pulses, which can be useful for a wide range of laser applications.

Keywords: pulse stretching; spatiotemporal shaping; ultrashort pulse trains; ultrafast imaging; burst laser ablation; transmission spectroscopic imaging.

Received Aug. 9, 2023; revised manuscript received Nov. 21, 2023; accepted for publication Nov. 23, 2023; published online Dec. 15, 2023.

[DOI: 10.1117/1.APN.3.1.016002]

1 Introduction

The production of ultrashort pulse trains is important for various applications, such as laser ablation,[1–5] ultrafast imaging,[6–10] and acoustic wave generation.[11] Laser-processing methods using pulse trains, such as double-pulse processing[1,4] and burst processing,[2,3,5] have been widely applied to improve processing accuracy and efficiency. In ultrafast imaging, pulse trains are used to capture the spatiotemporal dynamics of the optical properties of target objects.[6–10] In acoustic wave generation, multicycle acoustic waves can be tuned in the GHz frequency range by changing the time interval of the pulse train absorbed by the transducer.[11] One of the typical pulse trains contains pulses of different wavelengths. In this spectrally separated pulse train, the spatiotemporal profiles, such as pulse duration, and wavefront of each pulse can be individually modulated by pulse-shaping techniques using a diffraction grating, lens, and spatial light modulator (SLM).[12,13] Such spatiotemporal pulse shaping is crucial for the electron dynamics control in laser ablation,[14,15] fluorescence imaging,[16] and manipulation of terahertz signals,[17] among others. In addition, a spectrally separated pulse train is essential as a probe for sequentially timed all-optical mapping photography (STAMP),[6] which is a single-shot imaging technique that can capture two-dimensional burst images of ultrafast events. Therefore, producing spectrally separated ultrashort pulse trains and controlling their individual properties have promising implications in different applications.

Recently, the extension of the time interval of spectrally separated pulse trains to subnanoseconds or longer has attracted considerable attention. In particular, it is expected to pave the way for novel ablation techniques using ablation cooling and provide fundamental understanding of ultrafast phenomena through imaging with nanosecond time windows. One method for producing pulses with nanosecond intervals is a dispersive

*Address all correspondence to Keiichi Nakagawa, kei@bmpe.t.u-tokyo.ac.jp
†Present address: Research Institute for Electronic Science, Hokkaido University, Japan.

fiber-based device.[18–21] However, optical loss in fibers, which is a fundamental trade-off with pulse stretching, is severe at wavelengths other than the near-infrared communication bands. In addition, it is difficult to produce high-power pulses because of the nonlinear effects and optical damage to the fibers. In contrast, pulse-stretching methods that utilize the delay due to free space are not subject to these restrictions. Free-space angular-chirp-enhanced delay (FACED)[22] can produce pulse trains with subnanosecond or longer time intervals and has been used for ultrafast imaging.[22,23] FACED enables the illumination of an area spread out into a line shape with GHz burst pulses without significant optical loss. In contrast, its optical configuration does not allow the illumination of a specific area with all wavelength components of the burst pulses or their coaxialization. This is because, within each of the burst pulses produced by FACED, all wavelength components exhibit wavelength-dependent divergence and propagate in different directions. In applications such as laser processing and ultrafast imaging, there are many instances where the illumination of a point or circular area or the illumination from a single direction is necessary. In these cases, the spatial dispersion must be suppressed by sacrificing the bandwidth of each pulse, which inevitably results in optical losses. As methods to overcome this problem, a spectrum circuit[24] and recirculation-filtering method[25] are used for producing pulse trains with nanosecond intervals. However, the optical configuration, where the pulses circulate among four and three mirrors, respectively, cannot achieve subnanosecond time intervals. Meanwhile, a grating-based stretcher with an additional adjustable delay between subpulses[26] can produce spatially nondispersive pulse trains with subnanosecond intervals. However, the number of mirrors increases with the number of pulses, which inevitably complicates the optical system. Therefore, the easy production of spatially nondispersive and spectrally separated GHz burst pulses remains a challenge.

In addition, independent control of the spatial profiles of the GHz burst pulses has not been achieved with these burst pulse production systems. Individual pulse shaping of GHz burst pulses has the potential for pulse-by-pulse optimization in ablation and probing. Particularly, this would improve the accuracy and efficiency of burst-processing techniques. However, the conventional burst-pulse production systems require a pulse-shaping system using a diffraction grating, lens, and SLM to achieve individual shaping, which inevitably complicates and enlarges the overall system. A burst-pulse production system that can internally modulate the spatial profile of each pulse without adding the entire pulse shaping system provides a possible solution to address this.

In this study, we propose a spectrum shuttle as a method to produce pulse trains with subnanosecond to nanosecond intervals and individually shapable spatial profiles. First, we introduce pulse train production and individual spatial pulse shaping using a spectrum shuttle with an SLM. Subsequently, we demonstrate the production of spectrally separated pulse trains with time intervals of 100 ps to 3 ns. For imaging applications, we incorporate spectrum shuttles into two-color (TC)-STAMP to achieve ultrafast single-shot transmission spectroscopic imaging of laser ablation. Furthermore, we demonstrate the production of individually phase-modulated pulse trains as an example of spatial shaping.

2 Principles and Characteristics

2.1 Principles of Spectrum Shuttle

Figure 1(a) shows the overall optical configuration of a spectrum shuttle. An ultrashort pulse horizontally dispersed by a dispersion device (e.g., grating pair) is incident on a pair of parallel mirrors (mirrors 1 and 2) from above mirror 1. The incident

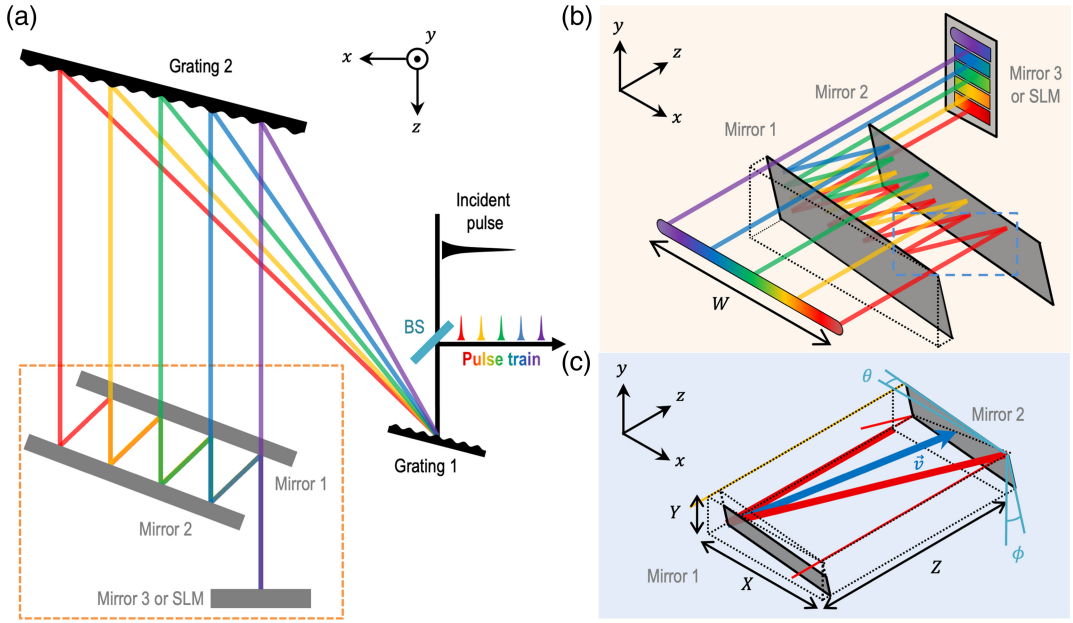

Fig. 1 Schematic of a spectrum shuttle. (a) Top view of the overall optical configuration. (b) Pulse separation by a pair of parallel mirrors (mirrors 1 and 2) indicated by the orange dashed square in (a). (c) Pulse traveling between parallel mirrors indicated in the blue dashed square in (b). BS, beam splitter; SLM, spatial light modulator.

light travels back and forth between the parallel mirrors, in which a daughter pulse with a specific wavelength component travels across the side of mirror 2 to mirror 3 (or an SLM) at every lap, whereas the pulse with the other wavelength components continuously travels between the parallel mirrors, as shown in Fig. 1(b). Consequently, the daughter pulses are vertically aligned and incident on mirror 3 (or the SLM). Here, when an SLM is used, each pulse can be individually spatially modulated. Subsequently, the reflected pulses return along their initial incoming paths and are picked off with a beam splitter (BS) as a spatially nondispersive and spectrally separated pulse train.

2.2 Number, Time Interval, and Duration of Daughter Pulses

In this section, we will discuss the principle of a spectrum shuttle based on ray tracing. A detailed derivation of the equations is provided in the Supplementary Material. As shown in Figs. 1(a) and 1(b), we take the x direction as the dispersion direction of the incident light, the z direction as the travel direction to mirror 3, and the y direction as perpendicular to the x and z directions. As shown in Fig. 1(c), let the distance between the parallel mirrors in the z direction be Z, and the rotation angles of the mirrors around the y- and x-axes be θ and ϕ, respectively. X and Y are the absolute shifts in the x and y directions in each lap, respectively. Here, the normal vector from mirror 1 to mirror 2, $\vec{v}$, is expressed by the following equation using the constant A:

$$\vec{v} = \left(\frac{X}{2}, \frac{Y}{2}, Z - \frac{X\tan\theta + Y\tan\phi}{2}\right) = A(\tan\theta, \tan\phi, 1). \quad (1)$$

Accordingly, the following equation is derived:

$$A = \frac{Z}{1 + (\tan\theta)^2 + (\tan\phi)^2}. \quad (2)$$

Therefore, X and Y are expressed as follows, respectively:

$$X = \frac{2\tan\theta}{1 + (\tan\theta)^2 + (\tan\phi)^2} Z, \quad (3)$$

$$Y = \frac{2\tan\phi}{1 + (\tan\theta)^2 + (\tan\phi)^2} Z. \quad (4)$$

X is equal to the width in the x direction of the daughter pulses extracted to mirror 3, and Y is equal to the interval in the y direction of the pulses on mirror 3, which should be longer than the beam diameter of the incident light, D. Using X, the number of the daughter pulses, M, is expressed as

$$M \approx \frac{W}{X}, \quad (5)$$

where W is the dispersion width by the dispersion device.

The time interval between the adjacent daughter pulses in the generated pulse train, T, is given as

$$T = T_{\mathrm{pm}} + T_{\mathrm{dis}}, \quad (6)$$

where T_{pm} is the temporal delay derived from the parallel mirrors, and T_{dis} is the delay derived from the other elements. In the parallel mirrors, the optical path length difference between the adjacent daughter pulses is represented by twice the length of the bold red line in Fig. 1(c), considering the paths before, and after the reflection on mirror 3. Therefore, T_{pm} is given as

$$T_{\mathrm{pm}} = \frac{2(2Z - X\tan\theta - Y\tan\phi)}{c} = \frac{2}{c}\left(Z + \sqrt{Z^2 - X^2 - Y^2}\right), \quad (7)$$

where c is the speed of light. Since $Z \geq \sqrt{X^2 + Y^2}$, T_{pm} has the minimum limit of

$$T_{\mathrm{pm}} \geq \frac{2\sqrt{X^2 + Y^2}}{c}. \quad (8)$$

When $T_{\mathrm{pm}} = 2\sqrt{X^2 + Y^2}/c$, the incident angle to the mirrors is 45 deg. In contrast, when $Z \gg X$, Y, the approximation is

$$T_{\mathrm{pm}} \approx \frac{4Z}{c}. \quad (9)$$

For example, when X and Y are 5 and 2 mm, respectively, T_{pm} according to Z is shown in Fig. 2(a). The minimum T_{pm} is 36 ps for $Z = 5.4$ mm, and an approximate proportionality is established with a delay in the range of nanoseconds. In addition, θ and ϕ according to T_{pm} are shown in Fig. 2(b). An optional delay of subnanoseconds to nanoseconds can be obtained by changing Z, where X and Y can be adjusted with θ and ϕ, respectively.

The delay derived from the elements other than parallel mirrors, T_{dis}, and the pulse duration of each daughter pulse, τ, are determined by the pulse duration of the light source and configuration of the dispersive elements. If a positively chirped pulse is used as a light source optimally compressed with a dispersion device in the spectral shuttle, T_{dis} can be reduced to zero and τ can be minimized. In this case, $T = T_{\mathrm{pm}}$, and the minimized pulse duration τ_{min} is

$$\tau_{\mathrm{min}} = \frac{k\lambda_{\mathrm{c}}^2}{c\Delta\lambda}, \quad (10)$$

where λ_{c} and $\Delta\lambda$ are the center wavelength and bandwidth of each daughter pulse, respectively, and k is a constant determined by the spectral waveform of the pulse. Assuming a square spectral waveform, k is 0.892. Although the pulse duration increases with the number of pulses because of the shortened bandwidth for each pulse, pulse trains with subpicosecond durations can be generated with optimal compression in the spectrum shuttle. In contrast, if the pulses are not optimally compressed, the temporal delay derived from elements other than parallel mirrors must be considered. In this case, T_{dis} is given as

$$T_{\mathrm{dis}} = |t(\lambda_{\mathrm{c}}) - t(\lambda_{\mathrm{c}}')|, \quad (11)$$

where $t(\lambda)$ is the delay derived from the elements other than parallel mirrors for each wavelength, λ; and λ_{c} and λ_{c}' are the center wavelengths of two adjacent daughter pulses. The pulse duration of each daughter pulse, τ, is similarly expressed using $t(\lambda)$ as follows:

$$\tau = \sqrt{[t(\lambda_{\mathrm{c}} + \Delta\lambda/2) - t(\lambda_{\mathrm{c}} - \Delta\lambda/2)]^2 + \tau_{\mathrm{min}}^2}. \quad (12)$$

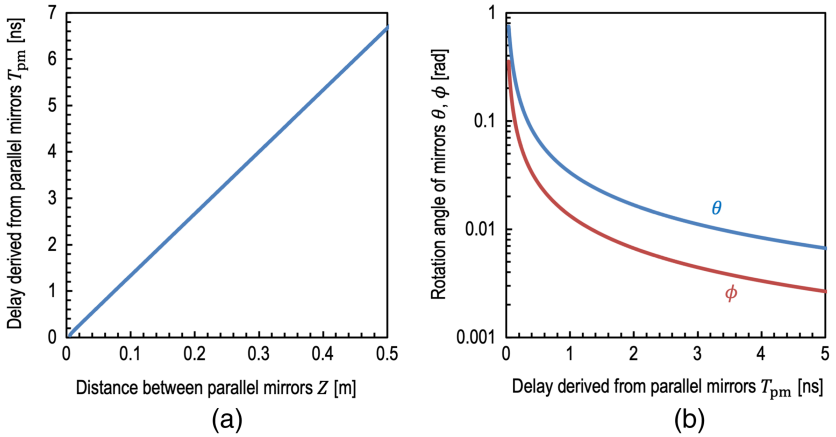

Fig. 2 Relationships of the basic parameters in a spectrum shuttle. (a) Variations of the temporal delay derived from the parallel mirrors, T_{pm}, with a distance between the parallel mirrors in the z direction, Z. (b) Rotation angles of the mirrors around the y and x axes, θ and ϕ, according to T_{pm}, respectively. Here, the absolute shifts in the x and y directions in each lap, X and Y are fixed at 5 and 2 mm, respectively, for both (a) and (b).

When a compressed pulse is used as the light source and a grating pair is used as the dispersion device, the delay other than that of the parallel mirrors is determined by the dispersion in the grating pair. In this case, $t(\lambda)$ is given as

$$t(\lambda) = \frac{2L[1 + (\lambda/d - \sin\alpha)\sin\alpha]}{c\cos\sin^{-1}(\lambda/d - \sin\alpha)}, \tag{13}$$

where d is the groove spacing of the diffraction gratings, α is the incident angle of the grating pair, and L is the distance between the gratings. In addition, the wavelength λ according to the x coordinate after diffraction by the second grating (grating 2), $\lambda(x)$, is given by the following equation when the point of incidence to the first grating (grating 1) is set to $x = 0$:

$$\lambda(x) = d\left[\sin\alpha + \sin\tan^{-1}\left(\frac{x/L + \sin\alpha}{\cos\alpha}\right)\right]. \tag{14}$$

A spectrum shuttle can independently control the number of pulses, M, and time interval, T, by adjusting the positions and angles of mirrors 1 and 2. The control of the pulse interval is independent of the pulse duration, which allows for longer intervals with short pulse duration.

2.3 Optical Loss

The optical loss is determined by four factors when a grating pair is used as the dispersion device, namely, the reflectivity of the mirrors, diffraction efficiency of the gratings, splitting by the BS, and splitting of the pulse at the edge of mirror 2, which occurs only at wavelengths that are incident on the edge. Let $x = x_0$ at the edge of mirror 2; the wavelength $\lambda(x)$ is split at the edge when x satisfies

$$|x - x_0 - mX| < \frac{D}{2}, \tag{15}$$

where m is any integer satisfying $0 \le m \le M - 2$, and D is the beam diameter of the incident light. These wavelengths span two daughter pulses and are partially lost because of the diffuse reflection and diffraction at the edge. This spanning should be noted in some spectroscopic techniques. If a spectral discretization is required, certain wavelengths can be shielded between mirrors 2 and 3, in exchange for additional optical loss.

For wavelengths without optical loss due to splitting at the edge of mirror 2, the optical loss at each wavelength, $\mathrm{Loss}(\lambda)$, can be expressed as

$$1 - \mathrm{Loss}(\lambda) = \Gamma^{4[m(\lambda)-1]}\Gamma'\eta_g^4 T_r R_e, \tag{16}$$

where Γ is the reflectivity of mirrors 1 and 2, Γ' is the reflectivity of mirror 3 (or the SLM), $m(\lambda)$'th is the pulse number that includes λ, η_g is the diffraction efficiency of the gratings, and T_r and R_e are the transmittance and reflectance of the BS, respectively. Here, the optical loss is independent of the time interval of a pulse train, and the use of optical elements with high efficiency enables a high throughput.

2.4 Spatial Shaping

Each daughter pulse can be individually spatially shaped using an SLM in the spectrum shuttle. A pixel resolution of the modulation in the y direction, N_y, is given as

$$N_y = \frac{D}{p}, \tag{17}$$

where p is the pixel pitch of the SLM. In contrast, a pixel resolution in the x direction, N_x, is given as

$$N_x = \frac{X}{p}. \tag{18}$$

Each wavelength component is subjected to different spatial modulation, unless the entire modulation in the x-axis direction is identical.

3 Experiments and Results

3.1 Production of Pulse Train

We constructed spectrum shuttles and demonstrated the production of GHz burst pulses. Two wavelength bands at ∼800 and 400 nm were chosen to represent the flexibility of the light source wavelength. A mode-locked Ti:sapphire laser with a chirped pulsed amplifier system (Astrella-USP-1K, Coherent) was used to generate a chirped pulse with a positive dispersion of 2 ps/nm, which was split by a BS before compression, and a compressed femtosecond laser pulse (duration of 35 fs). Both pulses have a center wavelength of 803 nm and a bandwidth of 35 nm (FWHM) at 100 Hz. A beta barium borate (BBO) crystal (BBO-1001H, EKSMA Optics, LT) was used to double the frequency of the femtosecond laser pulse. The chirped pulse before compression in the 800-nm band and second harmonic in the 400-nm band were used as the incident light to the spectrum shuttles after reducing their beam diameter to ∼2 mm. The incident lights were split using a 50:50 BS (BSW11 for 800 nm and BSW20 for 400 nm, Thorlabs) and dispersed by a grating pair (PC 1200 25 × 25 × 6 NIR/PC 1200 30 × 64 × 10 NIR for 800 nm and PC 2400 25 × 25 × 6 VIS/PC2400 50 × 50 × 6 VIS for 400 nm, Spectrogon, Sweden). In both bands, α and L were adjusted to 20 deg and 520 mm in the 800-nm band and 20 deg and 600 mm in the 400-nm band, respectively. Mirrors 1 and 2 (BBSQ-E03 for 800 nm and BBSQ-E02 for 400 nm, Thorlabs) were mounted on a kinematic mount (POLARIS-K1, Thorlabs) and goniometer stage for angle adjustment. In addition, mirror 1 was mounted on a single-axis stage for adjustment in the y direction, and mirror 2 was mounted on a dual-axis stage for adjustment in the x and z directions. The distance between grating 2 and mirror 3 was set to more than 250 mm to produce pulse trains with intervals of up to 3 ns. To adjust the delay time in the two bands, a single-axis stage in the z direction was attached to mirror 3 in the 400-nm band. For the parallel mirrors, we employed high-stability kinematic mounts and lockable stages to minimize optical system instability during experiments.

We first demonstrated the production of five pulses with an interval of 250 ps in the 800- and 400-nm bands. To measure the time-varying signal and spectrum of each daughter pulse, each pulse was extracted by a slit between mirrors 2 and 3. The time-varying signals of the pulse trains were measured using a fiber patch cable (M122L02, Thorlabs), a 33-GHz photodiode (DP070E1, Tektronix), and a 23-GHz oscilloscope (MSO72304DX, Tektronix); the results are shown in Figs. 3(a) and 3(b). The normalized spectra measured with a spectrometer (EPP2000 HR-NIR3 for 800 nm and HR-X-UV3 for 400 nm, SterllarNet) are shown in Figs. 3(c) and 3(d). Spectrally separated pulse trains are observed. The average pulse durations calculated from the measured spectra are 43 and 36 ps in the 800- and 400-nm bands, respectively. Figures 3(e) and 3(f) show the spectra when a portion of the wavelength component in each pulse was shielded by a blocker inserted between mirrors 2 and 3 from the negative direction of the x axis. The pulse trains were fully spectrally discretized. This discretization is effective in some spectral measurement techniques, including STAMP, where the overlap of the wavelength components between pulses can be a noise source.

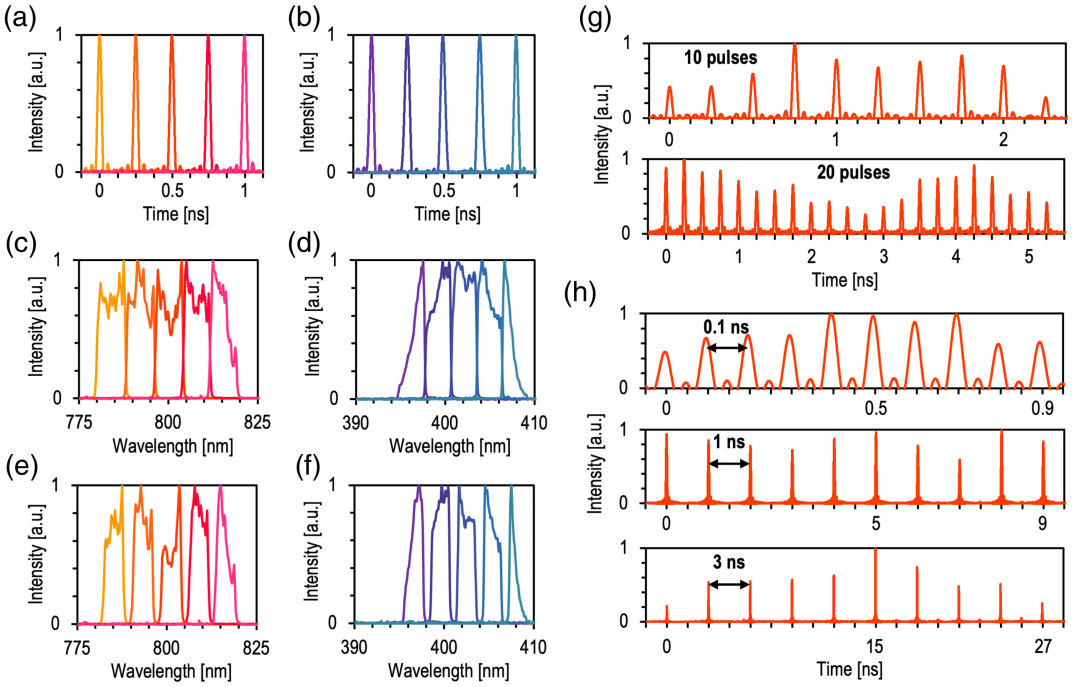

Fig. 3 Production of spectrally separated pulse trains by a spectrum shuttle. (a)–(d) Time-varying signals and spectra of five pulses with the intervals of 250 ps in the 800- and 400-nm bands. (e), (f) Spectra of the pulse trains discretized by shielding at one end between mirrors 2 and 3. (g), (h) Time-varying signals when the number or time interval of the pulses is changed in the 800-nm band.

Subsequently, the number and time interval of daughter pulses were changed in the 800-nm band to demonstrate the flexibility of the spectrum shuttle. Figure 3(g) shows the time-varying signals when the number of pulses was increased to 10 and 20 at an interval of 250 ps. Figure 3(h) shows the signals when the time interval of 10 daughter pulses was changed to 0.1, 1.0, and 3.0 ns. Note that the pulse distortion and artifacts beside the pulses are due to the electronic measurement using the oscilloscope with an analog bandwidth of 23 GHz and a sample rate of 100 G samples/s. In a spectrum shuttle, GHz burst pulses with the desired number and time interval can be generated by adjusting the angles and positions of the parallel mirrors. The production of a large number of pulses with longer intervals requires a high parallelism of the parallel mirrors, in which precision mirrors and their mounts with a high angular resolution can be effectively applied.

3.2 *Demonstration of Single-Shot Spectroscopic Imaging*

One of the applications of the pulse trains produced by a spectrum shuttle is ultrafast imaging with a time window in the range of subnanoseconds to nanoseconds. To demonstrate this application of the pulse trains, we applied them to TC-STAMP[27] and conducted single-shot transmission spectroscopic imaging of the subnanosecond dynamics of laser ablation. TC-STAMP is an ultrafast single-shot spectroscopic imaging technique based on the STAMP systems in two wavelength bands, which enables the analysis of wavelength-dependent parameters, such as absorption, scattering, and diffraction. Although the spectral properties of a laser ablation plasma have been acquired with a picosecond time window, the extension of the time window to the nanosecond scale will broaden the scope of analysis of ultrafast phenomena. In TC-STAMP, the stretched fundamental and second-harmonic pulses of the same light source are used as probe pulses. Here, we demonstrated TC-STAMP imaging with a time window extended to 1 ns using spectrum shuttles for the pulse stretching in two bands. A spectrum shuttle is advantageous in STAMP imaging using light sources with narrow bandwidths or low intensities, including second harmonics, because the sacrifice of the bandwidth in pulse stretching needs to be suppressed.

Figure 4(a) shows the experimental setup. We used pulse trains with the interval of 250 ps in the 800- and 400-nm bands as probes. The two pulse trains were coaxialized by a dichroic mirror (DM; DMLP425, Thorlabs) and simultaneously passed through the imaging area with the delay time adjusted by the stage of mirror 3 in the 400-nm spectrum shuttle. The pulse trains were then split by a DM (DMLP425R, Thorlabs) after the objective lens (M-PLAN APO SL 20X, Mitutoyo, Japan). Subsequently, the spectrally separated pulses in each band were split by the optical system utilizing spectral filtering[28] to image the pulses on the different areas of the image sensor (ORCA-Flash4.0 V3, Hamamatsu Photonics, Japan). The spectral filtering system consists of a diffractive optical element (DOE) to divide a pulse into five daughter pulses, a bandpass filter (BPF) to select different wavelength components, and a lens for imaging. In the 800-nm band, a DOE (DE 224, HOLOEYE, DE)

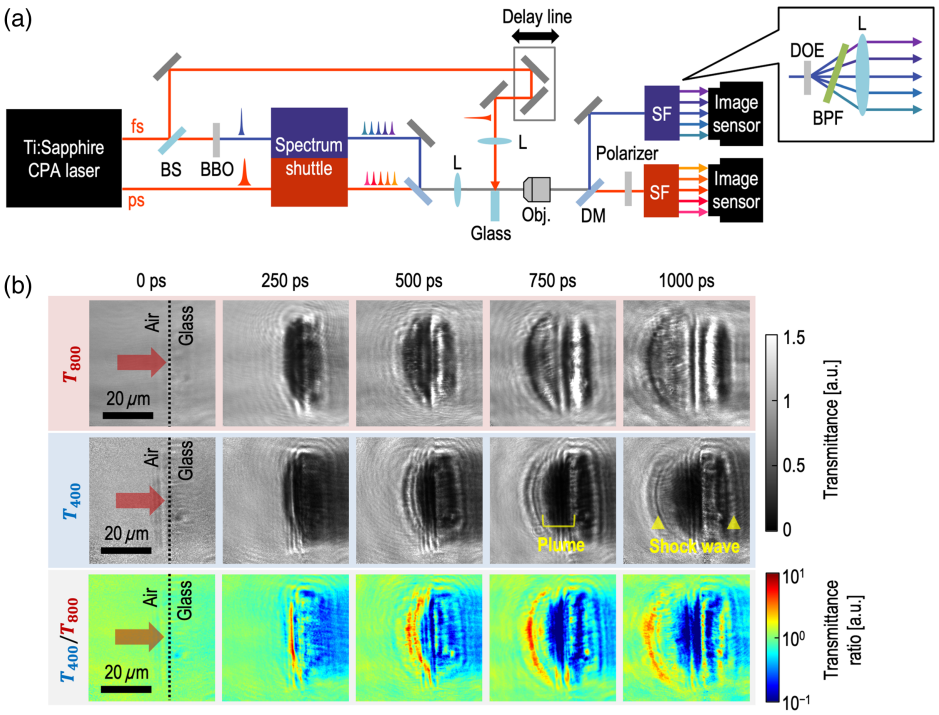

Fig. 4 Single-shot transmission spectroscopic imaging of laser ablation dynamics using pulse trains produced by spectrum shuttles in the 800- and 400-nm bands as probes. (a) Experimental setup. (b) Two-color transmittance distributions, T_{800} and T_{400}, and transmittance ratio between two wavelength bands, T_{400}/T_{800}, during the laser ablation dynamics. BS, beam splitter; BBO, beta barium borate; DM, dichroic mirror; L, lens; Obj., objective lens; SF, spectral filtering; DOE, diffractive optical element; BPF, bandpass filter.

with a diffraction angle of 8.2 deg, BPF (ZX000167, IRIDIAN, Canada) with a center wavelength of 830 nm and bandwidth of 2.2 nm, and lens with a focal length of 40 mm were used. In the 400-nm band, a DOE (DE-R 223, HOLOEYE, DE) with a diffraction angle of 5.1 deg, a BPF (416.06-0.5 OD6, Alluxa) with a center wavelength of 416.05 nm and bandwidth of 0.5 nm, and a lens with a focal length of 60 mm were used. The average exposure time for each frame, as calculated from the pulse stretching and BPF bandwidth, was 14 and 10 ps for the 800- and 400-nm band, respectively. As an excitation pulse, we used a femtosecond laser pulse in the 800-nm band split by a BS before the incidence on the BBO crystal. After passing through an optical delay line to adjust the delay time, the pulse was focused onto the surface of a 50-μm thick glass plate with a fluence of 40 J cm^{-2} by a lens with a focal length of 200 mm. The delay time was adjusted to allow the focused excitation pulse to coincide with the incidence of the first pulses of the two pulse trains. All pulses were extracted by mechanical shutters, and the laser ablation dynamics were captured by synchronized image sensors. In the 800-nm band STAMP, the excitation light scattering was removed by the polarizer (VISIR CW02, CODIXX AG, DE). Subsequently, we acquired the transmittance distribution of each frame in two bands by dividing the captured image by a previously captured reference image.

Figure 4(b) shows the transmittance distributions in the 800- and 400-nm band, T_{800} and T_{400}, respectively, during the laser ablation dynamics. The plasma plume evolved 1 ns after ablation. In addition, shock waves were generated and evolved in air and glass after 500 ps. The transmittance is affected by various factors, including electron absorption, scattering of heavy particles, and diffraction due to the refractive index distribution of plasmas and shock waves, which have different properties, depending on the wavelength. To highlight these spectral characteristics, the transmittance ratio between the two wavelength bands, T_{400}/T_{800}, is shown in Fig. 4(b). In the plasma plume, T_{400}/T_{800} decreased after 750 ps. This is presumably attributed to the dominance of the wide scattering by the heavy particles in short wavelengths, instead of the high absorption by the dense electrons in long wavelengths. The lower transmittance in the 400-nm band in the glass can be ascribed to the particle scattering. In contrast, the transmittance gradient at the shock wavefront in air is larger in the 800-nm band owing to large diffraction at long wavelengths. Therefore, TC-STAMP imaging with an extended time window was realized using spectrum shuttles, which allow for the detailed analysis of the spectral properties of ultrafast phenomena.

3.3 Demonstration of Individual Pulse Shaping

We next demonstrated spatial pulse shaping in the 800-nm spectrum shuttle by replacing mirror 3 with an SLM (SLM-100, Santec, Japan). Among the five daughter pulses generated with the interval of 250 ps by the spectrum shuttle, only the third pulse was independently modulated by the SLM, as shown in Fig. 5(a). Two different phase modulations were conducted. The first phase pattern was tilted in the y direction, which tilts the wavefront of the incident beam, thereby shifting the y axis during propagation and focusing. The second phase pattern includes a π step that splits the incident beam into two equal regions. This modulation can produce dual-peak pulses, which are applied to metal nanowire patterning.[29] We detected the beam profiles of the third pulse under three conditions: when the phase pattern is originally flat, has a gradient of $2\pi/3$ rad/mm, and has a step of π, as shown in Fig. 5(b). Under each condition, the third pulse was extracted by the slit between mirror 2 and the SLM in the spectrum shuttle and detected by an image sensor (ORCA-Flash4.0 V3, Hamamatsu Photonics, Japan) installed at a position where the third pulse propagated at ~1700 mm from the SLM.

Figure 5(c) shows the detected beam profiles of the modulated third pulse and average intensities of the pulses in the range of 2 mm. For the pattern with a gradient of $2\pi/3$ rad/mm, the center of gravity of the pulse shifted by 0.53 mm from the original position. Under a pattern with a step of π, a pulse with two peaks with a distance of 1.93 mm was produced. A daughter pulse can be individually modulated to these different profiles. The individual spatial shaping of the daughter pulses can greatly

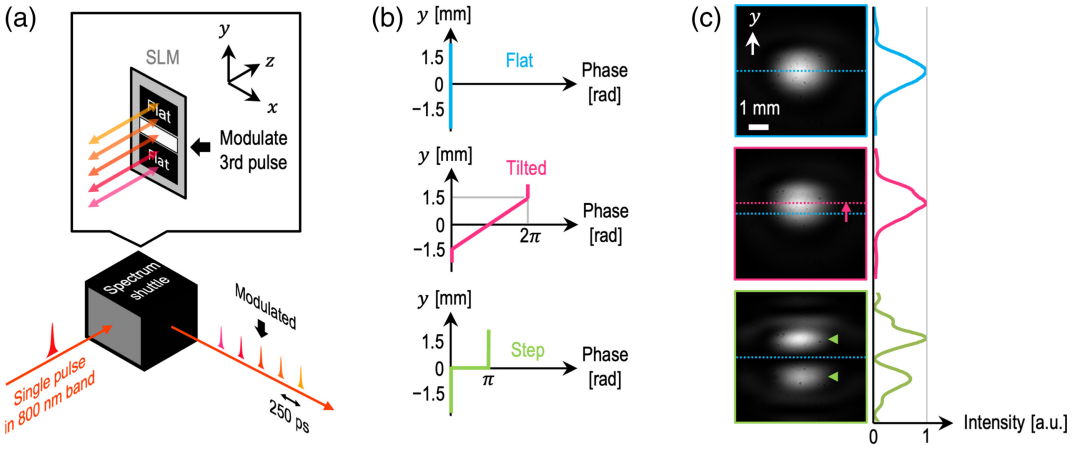

Fig. 5 Production of individually spatially shaped pulse trains by a spectrum shuttle with an SLM. (a) Experimental setup for modulating the third pulse only. (b) Phase patterns of the third pulse modulated by the SLM. (c) Beam profiles of the pulse propagated at ~1700 mm from the SLM under three conditions. On the right side, the average intensities of the pulses in the range of 2 mm at each y coordinate are shown.

increase the variety of the pulse trains, which is expected to allow pulse-by-pulse optimization for various applications, including ablation and probing.

4 Conclusions

In this study, we demonstrated a pulse manipulation technique, referred to as a spectrum shuttle, to produce spectrally separated GHz burst pulses from an ultrashort pulse without deteriorating the spectral components. A spectrum shuttle allows the use of pulse trains by adjusting the parallel mirrors with minimum time intervals of ∼30 ps. We experimentally obtained pulse trains with time intervals of 0.1 to 3 ns. Although the average pulse duration was 40 ps in the experiment owing to the temporal dispersion of the grating pair, adding a conventional pulse compressor using a diffraction grating and lens[30] either before or after the spectrum shuttle can bring the pulse duration of the burst pulses closer to the Fourier limit. The applicability of the produced GHz burst pulses was demonstrated by an ultrafast transmission spectroscopic imaging of a laser ablation with a time window of 1 ns. Burst pulses with a time interval of 250 ps in the 800- and 400-nm bands produced by the spectrum pulses were used as probes. The use of the spectrum shuttle in ultrafast imaging enables a multifaceted analysis of ultrafast phenomena. Furthermore, we achieved the production of individually spatially shaped GHz burst pulses using the spectrum shuttle incorporated with an SLM, which allows unprecedented spatiotemporal manipulation of GHz burst pulses. Therefore, the proposed spectrum shuttle has strong potential as a pulse manipulation technique for various applications, such as burst laser ablation and ultrafast imaging.

Disclosures

The authors declare no conflicts of interest.

Code and Data Availability

Data underlying the results presented in this paper are available from the corresponding author upon reasonable request.

Acknowledgments

This work was supported by MEXT Quantum Leap Flagship Program (MEXT Q-LEAP) (Grant No. JPMXS0118067246). K.S. was supported by JST ACT-X (JPMJAX22K8). Y.I. and A.I. were partly supported by JST PRESTO (JPMJPR2003 and JPMJPR1902, respectively). K.N. was partly supported by JST FOREST (JPMJFR215C).

References

1. M. Barberoglou et al., "The influence of ultra-fast temporal energy regulation on the morphology of Si surfaces through femtosecond double pulse laser irradiation," *Appl. Phys. A* **113**(2), 273–283 (2013).
2. C. Kerse et al., "Ablation-cooled material removal with ultrafast bursts of pulses," *Nature* **537**(7618), 84–88 (2016).
3. K. Mishchik et al., "High-efficiency femtosecond ablation of silicon with GHz repetition rate laser source," *Opt. Lett.* **44**(9), 2193–2196 (2019).
4. M. Spellauge et al., "Influence of stress confinement, particle shielding and re-deposition on the ultrashort pulse laser ablation of metals revealed by ultrafast time-resolved experiments," *Appl. Surf. Sci.* **545**, 148930 (2021).
5. Y. Zhang et al., "Extremely regular periodic surface structures in a large area efficiently induced on silicon by temporally shaped femtosecond laser," *Photonics Res.* **9**(5), 839–847 (2021).
6. K. Nakagawa et al., "Sequentially timed all-optical mapping photography (STAMP)," *Nat. Photonics* **8**(9), 695–700 (2014).
7. A. Ehn et al., "FRAME: femtosecond videography for atomic and molecular dynamics," *Light Sci. Appl.* **6**(9), e17045 (2017).
8. C. Guanghua et al., "All-optical coaxial framing photography using parallel coherence shutters," *Opt. Lett.* **42**(3), 415–418 (2017).
9. S. Yeola, D. Kuk, and K.-Y. Kim, "Single-shot ultrafast imaging via spatiotemporal division of femtosecond laser pulses," *J. Opt. Soc. Am. B* **35**(11), 2822–2827 (2018).
10. J. Liang and L. V. Wang, "Single-shot ultrafast optical imaging," *Optica* **5**(9), 1113–1127 (2018).
11. C. Klieber et al., "Narrow-band acoustic attenuation measurements in vitreous silica at frequencies between 20 and 400 GHz," *Appl. Phys. Lett.* **98**(21), 211908 (2011).
12. A. M. Weiner, "Femtosecond pulse shaping using spatial light modulators," *Rev. Sci. Instrum.* **71**(5), 1929–1960 (2000).
13. T. Feurer et al., "Multidimensional control of femtosecond pulses by use of a programmable liquid-crystal matrix," *Opt. Lett.* **27**(8), 652–654 (2002).
14. L. Jiang et al., "Electrons dynamics control by shaping femtosecond laser pulses in micro/nanofabrication: modeling, method, measurement and application," *Light Sci. Appl.* **7**(2), 17134 (2018).
15. P. S. Salter and M. J. Booth, "Adaptive optics in laser processing," *Light Sci. Appl.* **8**(1), 110 (2019).
16. S. Chu et al., "Optimizing two-photon fluorescence of Coumarin dye by combined temporal-spatial pulse shaping," *Opt. Commun.* **284**(16–17), 4070–4072 (2011).
17. T. Feurer et al., "Spatiotemporal coherent control of lattice vibrational waves," *Science* **299**(5605), 374–377 (2003).
18. M. A. Muriel, J. Azaña, and A. Carballar, "Real-time Fourier transformer based on fiber gratings," *Opt. Lett.* **24**(1), 1–3 (1999).
19. K. Goda, K. K. Tsia, and B. Jalali, "Serial time-encoded amplified imaging for real-time observation of fast dynamic phenomena," *Nature* **458**(7242), 1145–1149 (2009).
20. Y. Jiang, S. Karpf, and B. Jalali, "Time-stretch LiDAR as a spectrally scanned time-of-flight ranging camera," *Nat. Photonics* **14**(1), 14–18 (2020).
21. R. Liao et al., "Chromo-modal dispersion for optical communication and time-stretch spectroscopy," *Opt. Lett.* **46**(3), 500–503 (2021).
22. J. -L. Wu et al., "Ultrafast laser-scanning time-stretch imaging at visible wavelengths," *Light Sci. Appl.* **6**(1), e16196 (2017).
23. H. Nemoto, T. Suzuki, and F. Kannari, "Extension of time window into nanoseconds in single-shot ultrafast burst imaging by spectrally sweeping pulses," *Appl. Opt.* **59**(17), 5210–5215 (2020).
24. T. Saiki et al., "Spectrum circuit for producing spectrally separated nanosecond pulse train in free space," in *CLEO: Sci. and Innov., OSA Tech. Digest*, Optica Publishing Group, Washington, D.C., p. SM1H.5 (2020).
25. A. Honda et al., "Development of sub-Gfps ultrafast snapshot imaging system based on recirculation filtering of ultrashort optical pulses," in *CLEO: Sci. and Innov., Tech. Digest Ser.*, Optica Publishing Group, San Jose, California, p. STh4L.7 (2022).
26. M. Touil et al., "Acousto-optically driven lensless single-shot ultrafast optical imaging," *Light Sci. Appl.* **11**(1), 66 (2022).
27. K. Shimada et al., "Single-shot transmission spectroscopic imaging by two-color stretched pulses," *Rev. Laser Eng.* **49**(4), 240–244 (2021).
28. T. Suzuki et al., "Sequentially timed all-optical mapping photography (STAMP) utilizing spectral filtering," *Opt. Express* **23**(23), 30512–30522 (2015).

29. A. Wang et al., "Mask-free patterning of high-conductivity metal nanowires in open air by spatially modulated femtosecond laser pulses," *Adv. Mater.* **27**(40), 6238–6243 (2015).
30. O. Martinez, "3000 times grating compressor with positive group velocity dispersion: application to fiber compensation in 1.3–1.6 μm region," *IEEE J. Quantum Electron.* **23**(1), 59–64 (1987).

Keitaro Shimada received his MS degree in bioengineering from the University of Tokyo, Tokyo, Japan, in 2022. He is currently a PhD student at the University of Tokyo. His research interests are ultrafast optical imaging and its diverse applications.

Ayumu Ishijima received his PhD in precision engineering from the University of Tokyo, Tokyo, Japan, in 2018. He is currently an assistant professor at Hokkaido University, Hokkaido, Japan. His research interests are biophotonics, bioacoustics, and ultrasonics.

Takao Saiki received his MS degree in precision engineering from the University of Tokyo, Tokyo, Japan, in 2021. He is currently a PhD student at the University of Tokyo. His research interests are ultrafast optical imaging and its biomedical applications.

Ichiro Sakuma received his PhD in precision machinery engineering from the University of Tokyo, Tokyo, Japan, in 1989. He is currently a professor at the University of Tokyo. His research interests include biomedical instrumentation, simulation of biomedical phenomena, computer-assisted intervention, and surgical robotics.

Yuki Inada received his PhD in electrical engineering from the University of Tokyo, Tokyo, Japan, in 2014. He is currently an associate professor at Saitama University, Saitama, Japan. His research interests are discharge plasma engineering and optical engineering.

Keiichi Nakagawa received his PhD in precision engineering from the University of Tokyo, Tokyo, Japan, in 2014. He is currently an associate professor at the University of Tokyo. His research interests are biomedical engineering, precision engineering, and optical engineering.